Chapter 2

Planar Optics

Since J. Jahns et al. proposed the planar integration of free-space optical components in 1989, numerous researches on planar-integrated free-space optics (planar optics) and their applications emerged. According to J. Jahns' originality, the idea of planar optics is to fold the optical signal as a zigzag path which bounces between the two mirrored surfaces of a planar substrate, as illustrated in Fig. 2-1 (a). The substrate shall be a homogeneous block with little absorption while the optical components are distributed over the surfaces of substrate. By using micro-fabrication techniques, an integrated optics can be realized. Before, because of the applications to optical communication and computation, the input/output terminals of planar optics were typically located at left and right ends of the substrate. However, for the usage in flat panel displays (FPDs), the planar optics is extended as another scheme of bottom-input and top-output, as shown in Fig. 2-1 (b); examples will be given in Chapter 4 and Chapter 5.

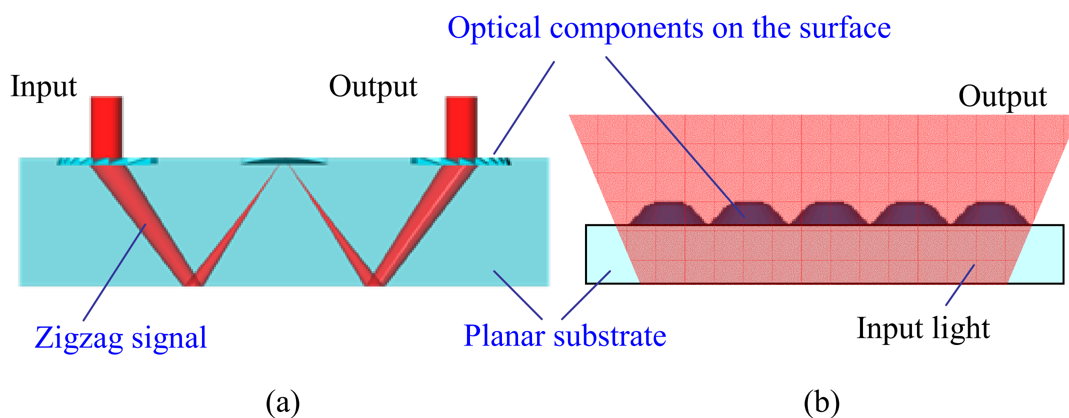

Fig. 2-1 Concepts of planar optics: (a) typical and (b) extended forms.

In this chapter, the theories of aberration compensation and efficiency in typical planar optics will be elucidated first. Then the modeling of planar optics will be introduced in terms of the refractive optical element (ROE) and the diffractive optical element (DOE), followed by the related fabrication techniques. Thence the main issue of planar optics caused by insufficient light efficiency as well as its solutions will be discussed.

2.1 Theories of typical planar optics

Compared with conventional free space optics, the typical planar optics has several characteristics, such as the oblique propagation and the preference of shallow-sag components. The formal characteristic causes aberrations, especially the astigmatism; therefore, the compensation theory will be discussed in the following sub-section. The later is due to the requirements of compactness and precise alignment, which standard semiconductor processes can offer. Then the shallow-sag and quantized components such as quantized DOEs are preferred. When a quantized DOE is adopted then one of the significant considerations will be the efficiency, whose formula will be given in section 2.1.2 as a reference.

2.1.1 Compensation of aberration

To compensate the aberrations of typical planar optics, we can start on the phase difference between the image and the object in a planar lens system. Consider that a planar optical lens, an object and an image locate at the plane of z = 0, (x_0, y_0, z_0) and (x_i, y_i, z_i), respectively (Fig. 2-2). The chief ray is assumed to be at the x-z plane and inclined by an angle θ with respect to the z axis. When the optical path is unfolded, the equivalent coordinates of the image is labeled as (x_1, y_1, z_1). For simplicity, y_0, y_i, and y_1 are assumed to be zero. Meanwhile, due to the paraxial approximation, we

assume: $x_0 = z_0\theta$ and $x_1 = z_1\theta$ with $z_0 < 0$ and $z_1 > 0$.

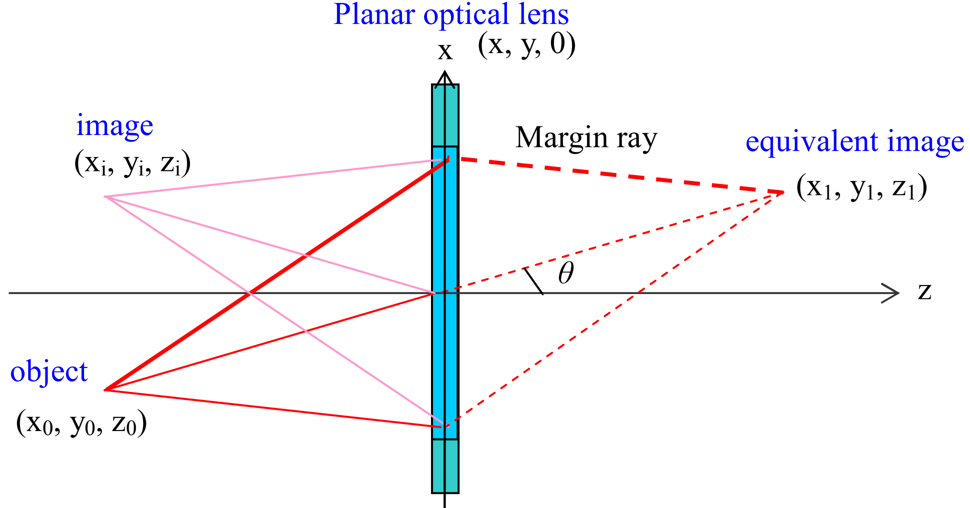

Fig. 2-2 Illustration of imaging function in a typical planar optical lens.

Then, if the margin ray intersects with the lens at the point of (x, y, 0), the phase difference between the image and object along the margin ray can be derived:

$$\Phi_m = \frac{2\pi}{\lambda}\left(\sqrt{(x_0 - x)^2 + (y_0 - y)^2 + (z_0 - 0)^2} + \sqrt{(x_1 - x)^2 + (y_1 - y)^2 + (z_1 - 0)^2}\right)$$
$$= \frac{2\pi}{\lambda}\left(\sqrt{(x - z_0\theta)^2 + y^2 + z_0^2} + \sqrt{(x - z_1\theta)^2 + y^2 + z_1^2}\right) \qquad (2\text{-}1)$$

According to Taylor series,

$$\sqrt{1+a} = 1 + \frac{a}{2} - \frac{a^2}{8}\cdots \qquad (2\text{-}2)$$

The high order terms can be neglected due to the paraxial approximation. Then eq. (2-1) becomes:

$$\Phi_m = \frac{2\pi}{\lambda}\left(-z_0\sqrt{1 + \frac{(x - z_0\theta)^2 + y^2}{z_0^2}} + z_1\sqrt{1 + \frac{(x - z_1\theta)^2 + y^2}{z_1^2}}\right)$$
$$\cong \frac{2\pi}{\lambda}\left(-z_0\left(1 + \frac{(x - z_0\theta)^2 + y^2}{2z_0^2} - \frac{\left((x - z_0\theta)^2 + y^2\right)^2}{8z_0^4}\right) + \right.$$
$$\left. z_1\left(1 + \frac{(x - z_1\theta)^2 + y^2}{2z_1^2} - \frac{\left((x - z_1\theta)^2 + y^2\right)^2}{8z_1^4}\right)\right) \qquad (2\text{-}3)$$

The 2nd and 5th terms with the denominator order of z lead to the 1st order phase difference, while the 3rd and 6th terms with the denominator order of z^3 result in the 3rd order phase difference. For the chief ray of typical planar optics, its phase difference between the image and object shall be:

$$\begin{aligned}\Phi_c &= \frac{2\pi}{\lambda}\left(\sqrt{x_0^2+z_0^2}+\sqrt{x_1^2+z_1^2}\right)\\ &= \frac{2\pi}{\lambda}\left(\sqrt{(z_0\theta)^2+z_0{}^2}+\sqrt{(z_1\theta)^2+z_1{}^2}\right)\\ &= \frac{2\pi}{\lambda}\left(-z_0\sqrt{1+\theta^2}+z_1\sqrt{1+\theta^2}\right)\\ &\cong \frac{2\pi}{\lambda}\left(-z_0(1+\frac{\theta^2}{2}-\frac{\theta^4}{8})+z_1(1+\frac{\theta^2}{2}-\frac{\theta^4}{8})\right)\end{aligned} \tag{2-4}$$

The difference between Φ_m and Φ_c causes aberrations, which can then be calculated from eqs (2-3) and (2-4). The first order of phase difference Φ_1 shall be contributed by the conventional lens profile. Assume that the focal length of lens is f; then Φ_1 can be derived as:

$$\begin{aligned}\Phi_1 &= \frac{2\pi}{\lambda}\left(\frac{1}{z_1}-\frac{1}{z_0}\right)\left(\frac{x^2+y^2}{2}\right)\\ &= \frac{\pi}{\lambda}\frac{x^2+y^2}{f} \qquad where\ \frac{1}{f}=\frac{1}{z_1}-\frac{1}{z_0}\end{aligned} \tag{2-5}$$

On the other hand, the 3rd order of phase differences causes the Seidel aberrations: spherical aberration, coma and astigmatism; they are:

$$\begin{aligned}\Phi_{sph} &= \frac{\pi}{4\lambda}\left(\frac{1}{z_0{}^3}-\frac{1}{z_1{}^3}\right)\left(x^4+2x^2y^2+y^4\right)\\ \Phi_{com} &= \frac{-\pi\theta}{\lambda}\left(\frac{1}{z_0{}^2}-\frac{1}{z_1{}^2}\right)\left(x^3+xy^2\right)\\ \Phi_{ast} &= \frac{\pi\theta^2}{2\lambda}\left(\frac{1}{z_0}-\frac{1}{z_1}\right)\left(3x^2+y^2\right)\end{aligned} \tag{2-6}$$

Due to the oblique propagation in a typical planar optical system, the significance of the above aberrations increases with the contribution of θ; that is, astigmatism affects the image quality more than other aberrations. Therefore, at least astigmatism shall be compensated. For an astigmatism-free planar optical lens, its profile shall compensate the phase difference through an elliptical profile:

$$\begin{aligned} \Phi' &= \frac{\pi}{\lambda}\left(\frac{x^2}{f_x}+\frac{y^2}{f_y}\right) \\ &= \Phi_1 + \Phi_{ast} \end{aligned} \tag{2-7}$$

According to eqs (2-5) to (2-7), one can derive:

$$\Phi' = \frac{\pi}{\lambda}\left(\frac{x^2}{f}\cdot\left(1-\frac{3\theta^2}{2}\right)+\frac{y^2}{f}\cdot\left(1-\frac{\theta^2}{2}\right)\right) \tag{2-8}$$

Therefore, the compensated focal lengths of the x and y axes are:

$$\begin{aligned} f_x &= \frac{f}{1-\frac{3\theta^2}{2}} \cong \frac{f}{\cos^3\theta} \\ f_y &= \frac{f}{1-\frac{\theta^2}{2}} \cong \frac{f}{\cos\theta} \end{aligned} \tag{2-9}$$

The compensation of the other two aberrations can be realized by the design of the lens profile and the locations of object and image. According to the literature,[1] the compensation of astigmatism is sufficient for a typical planar optical system.

2.1.2 Efficiency of quantized diffractive optics

In this subsection, a linear grating with a period of p is considered as an example to derive the efficiency of DOEs. Assume that the grating is made of lossless material and has infinite one-dimensional periods with L quantized levels per period. Then, the transmittance function of $g(\mathrm{x}) = g(x+p)$ can be expressed as a Fourier series:

$$g(x)=\sum_{m=-\infty}^{\infty}A_m e^{j2\pi mx/p} \tag{2-10}$$

where A_m is the amplitude of the mth diffraction order and can be derived from:

$$A_m=\frac{1}{p}\int_0^p g(x)e^{-j2\pi mx/p}dx \tag{2-11}$$

As a result of the quantized profile of the designated grating, a non-absorbing grating has its mathematical transmittance function of:

$$g(x)=e^{-j\varphi(x)}=\sum_{q=0}^{L-1}e^{-j2\pi q/L}rect\left(\frac{x-\frac{qp}{L}-\frac{p}{2L}}{P/L}\right) \tag{2-12}$$

where $\varphi(x)$ is the phase function of $g(x)$, as shown in Fig. 2-3. Substitute eq. (2-12) into eq. (2-11):

$$\begin{aligned}A_m&=\frac{1}{p}\int_0^p\sum_{q=0}^{L-1}e^{-j2\pi q/L}\cdot rect\left(\frac{x-\frac{qp}{L}-\frac{p}{2L}}{p/L}\right)\cdot e^{-j2\pi mx/p}dx\\&=\frac{1}{p}\sum_{q=0}^{L-1}e^{-j2\pi q/L}\cdot\int_0^p rect\left(\frac{x-\frac{qp}{L}-\frac{p}{2L}}{p/L}\right)\cdot e^{-j2\pi mx/p}dx\end{aligned} \tag{2-13}$$

According to Fourier transform, the integration shall be:

$$\begin{aligned}\int_0^p rect\left(\frac{x-\frac{qp}{L}-\frac{p}{2L}}{p/L}\right)\cdot e^{-j2\pi mx/p}dx&=\frac{p}{L}\cdot sinc(\frac{p}{L}\cdot\frac{m}{p})\cdot\exp\left(-j2\pi m(\frac{q}{L}+\frac{1}{2L})\right)\\&=\frac{p}{L}\cdot sinc\left(\frac{m}{L}\right)\cdot e^{-j2\pi mq/L}\cdot e^{-j\pi m/L}\end{aligned} \tag{2-14}$$

where $\mathrm{sinc}(x)=\sin(\pi x)/\pi x$. Then, A_m can be derived as:

$$\begin{aligned}A_m&=\left(\frac{1}{L}\right)\cdot\sum_{q=0}^{L-1}e^{-j2\pi q/L}\cdot e^{-j2\pi mq/L}\cdot e^{-j\pi m/L}\cdot\mathrm{sinc}\left(\frac{m}{L}\right)\\&=e^{-j\pi m/L}\cdot\mathrm{sinc}\left(\frac{m}{L}\right)\cdot\left(\frac{1}{L}\right)\cdot\sum_{q=0}^{L-1}e^{-j2\pi q(1+m)/L}\end{aligned} \tag{2-15}$$

The summation over q yields non-zero results only when $q(1+m)/L$ is an integer. Then, the last two terms shall be:

$$\left(\frac{1}{L}\right)\cdot\sum_{q=0}^{L-1} e^{-j2\pi q(1+m)/L} = \begin{cases} 1 & q(1+m)/L \in Z \\ 0 & others \end{cases} \tag{2-16}$$

Equation (2-16) infers that only when m satisfies $1+m = 0, \pm L, \pm 2L$, the diffraction can occur. Thus, from eq. (2-15), the intensity of mth order diffraction $I_m = |A_m|^2$ is:

$$I_m = \mathrm{sinc}^2\left(\frac{m}{L}\right) \tag{2-17}$$

Consequently, the efficiency of mth order, defined as the ratio of the intensity I_m to the incident intensity that equals to the sum of all diffractive intensities ($\sum_{t=-\infty}^{\infty}|A_m|^2 = 1$), can be derived:

$$\eta_m = \frac{I_m}{\sum_{t=-\infty}^{\infty}|A_m|^2} = \mathrm{sinc}^2\left(\frac{m}{L}\right) \tag{2-18}$$

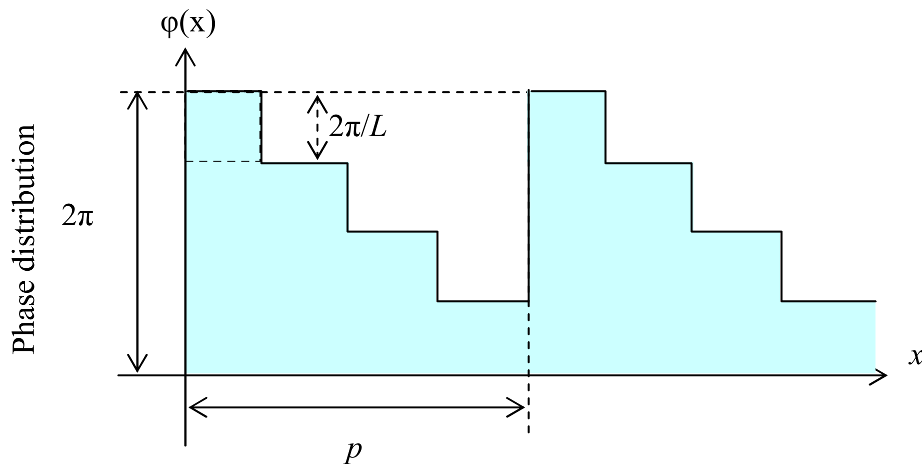

Fig. 2-3 Phase distribution of the quantized 1-D diffractive grating.

As for a quantized diffractive lens like a Fresnel zone plate (FZP), since the

transmittance function $g(x, y)$ is radial symmetry and periodic in r^2, $g(x, y)$ can be expressed as: $g(x, y) = g(x^2+y^2) = g(r^2) = g(r^2+r_p^2)$ with the period of r_p^2. Using the coordinate transform and following the above procedures, one can derive the same diffractive efficiency as in eq. (2-18). [2]

2.2 Modeling

Optical components can be simply classified into two groups of ROEs and DOEs, and so can the planar optics. The parameter used to distinguish between ROEs and DOEs is the feature size of the component. When the feature size is much larger than the wavelength, the component belongs to the ROE category and can be modeled by ray optics. Otherwise, the component shall be regarded as a DOE and modeled by wave optics.[3],[4]

2.2.1 Refractive optical element (ROE)

Although Maxwell's equations can thoroughly model an optical system, the calculation of a system with complex components takes long time and needs large memory space. In order to simplify the calculation, some appropriate approximations shall be taken. For a ROE in the planar optics, the ray optics, which regards light as rays independent of wavelength or polarization, is sufficient to model the behaviors of the light propagation as well as the interaction between the light and the ROE.

A typical planar optical device with ROEs can be expressed as a conventional free-space optical system by unfolding the optical path, as shown in Fig. 2-4. Then, the direction and the position of light can be calculated by the ray-tracing approach, including the linear propagation and the Snell's law:

$$n_1 \sin\theta_1 = n_2 \sin\theta_2 \qquad (2\text{-}19)$$

where n_1, n_2, θ_1, and θ_2 are the refractive indexes before and after the boundary

between media, the incident angle, and the refractive angle, respectively.

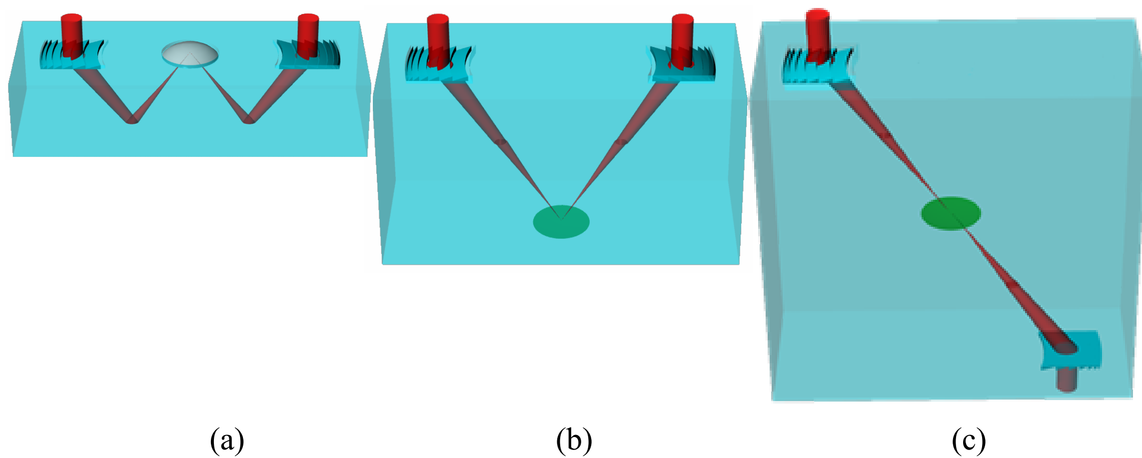

(a) (b) (c)

Fig. 2-4 Unfolded planar optics with (a) original, (b) half unfolded, and (c) fully unfolded optical paths.

1896

When the number of elements on a planar optical device increases to some extent, it becomes necessary to analyze such a device with the aid of computer programs. For the planar optics with ROEs, commercial softwares, such as OSLO, ASAP, LightTools, TracePro, ZEMAX, CODE 5 etc., or private programs based on ray tracing are useful to perform the modeling and the evaluation efficiently.

2.2.2 Modeling of Diffractive optical element (DOE)

Although the planar optics has the advantage of compact size due to the folded optical path, the thickness of every element can be further reduced by utilizing a DOE design. That is because a DOE can perform the function of the corresponding ROE and has a reduced thickness via phase quantization technique.[4],[5] Not only contributing to miniature devices, DOEs in planar optics are also adapted to the standard semiconductor fabrication processes, resulting in a specimen with good alignment and accurate profile. However, unlike the ROE, a DOE is a

wavelength-dependent device and the wave properties of light can not be neglected in the modeling. Consequently, the computational complexity is raised. To establish an efficient model, Kirchhoff approximation and Fresnel diffraction are utilized to analyze the functions of elements and the propagation of light, respectively, due to their proved sufficiency for modeling planar optical systems.[4]

Kirchhoff approximation assumes that the depth of profile in a DOE is very thin; then, the field of wave behind the DOE can be derived by the product of the field of incident wave and the complex surface profile of DOE. As shown in Fig. 2-5, the incident wave and the output wave are denoted to be U and U', respectively. The interaction between the light and the DOE is assumed to occur on the (x, y) plane; then, the function of the DOE, $F(x, y)$, will be:

$$F(x,y) = A(x,y)\exp(-i\varphi(x,y)), \tag{2-20}$$

where A is the amplitude term related to the absorption of the DOE; φ is the phase term related to the wavelength λ, the profile and the refractive index of the DOE. According to Kirchhoff approximation (thin element approximation), U' can be derived by:

$$U' = U(x,y) \cdot F(x,y). \tag{2-21}$$

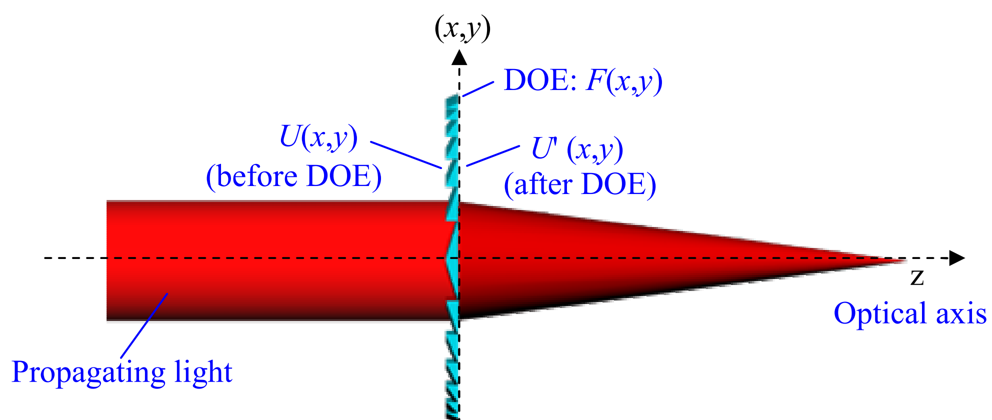

Fig. 2-5 Illustration of Kirchhoff approximation.

On the other hand, Fresnel diffraction approximation (paraxial approximation) is used to model the light propagation for a typical planar optical system. This approximation expresses the free-space propagation as a scalar form derived from Maxwell's equations and is valid for the small angle propagation (the angle between the direction of light and the optical axis is normally < 20° for glass substrate to keep the difference between paraxial and real refraction rays within 1°) [6]. Since the propagation of light in a typical planar optical system inclines usually less than 10° with respect to the z axis,[7] Fresnel diffraction approximation is appropriate for modelling the light propagation herein.

Consider the field U' at the plane just behind the DOE as the original field of propagation, as shown in Fig. 2-6. The original and the destination planes are labelled as $z = z_0$ and $z = z_1$, respectively. According to Fresnel diffraction approximation, the field U_1 at the destination (x_1, y_1, z_1) can be derived by the Fourier transform:

$$U_1(x_1, y_1, z_1) = \frac{e^{ik(z_1 - z_0)}}{i\lambda(z_1 - z_0)} \iint U'(x, y, z_0) \exp\left(\frac{i\pi[(x_1 - x)^2 + (y_1 - y)^2]}{\lambda(z_1 - z_0)} \right) \cdot dxdy \quad (2\text{-}22)$$

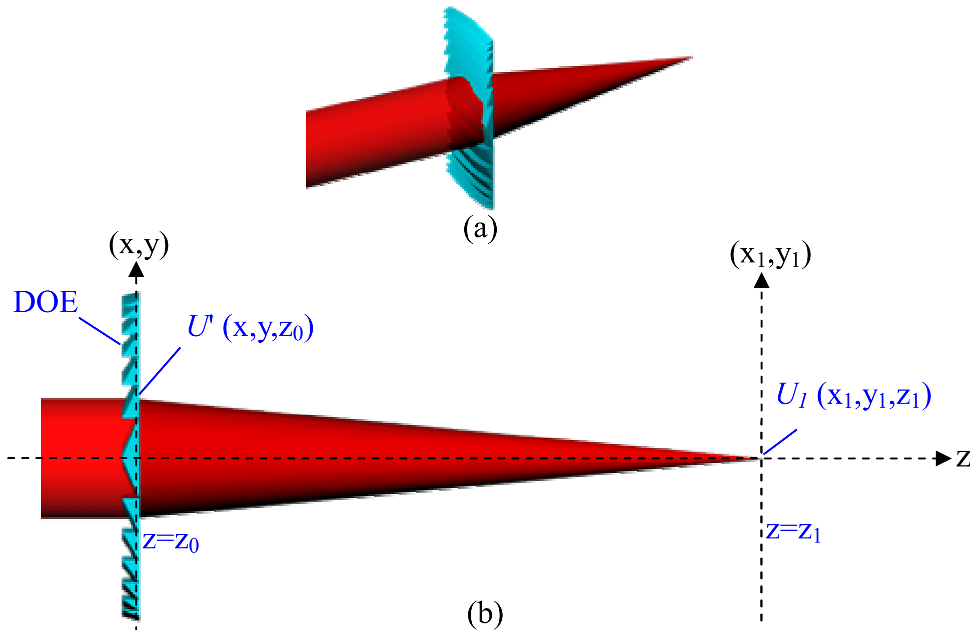

Fig. 2-6 Light propagation in a typical planar optical system: (a) perspective and (b) side views.

As the extended planar optics is concerned, the assumptions of thin elements and paraxial propagation might be invalid for some planar DOEs. Then, the rigorous modelling methods, such as rigorous coupled-wave analysis (RCWA) and finite difference time domain method (FDTD), derived from Maxwell's equations without approximation are necessary. Besides programs written by designers privately, commercial tools like GSOLVER and FDTD Solutions are available to simulate such DOEs. An example of patched wire-grid polarizer, a DOE beyond the Kirchhoff approximation and the Fresnel diffraction regimes, will be presented in Chapter 5.

2.2.3 Design of Diffractive optical element (DOE)

After the discussion of modeling planar optical DOEs, the design principle will be described in this section. Compared to a ROE or a 1-dimensional DOE grating, designing a 2-dimensional DOE, such as a lens, is rather complicated. Here, a DOE lens design will be discussed as an example.

Consider a DOE lens with a focal length of f, as shown in Fig. 2-7. The profile of the lens is quantized by L levels. Each level refers to a main phase order m, defined as the integral multiples of wavelength, and a sub-phase order l, defined as the remained phase module. Then, for a DOE lens (the refractive index = n), the phase difference φ between the central beam and the beam intercepting at the (l, m) level is:

$$\varphi = \frac{2\pi \cdot l}{L} + 2\pi \cdot m, \qquad l = 0,1,2...(L-1)\,. \tag{2-23}$$

Assume that the (l, m) level offers a path difference of $p_{l,m}$. φ can be also expressed as:

$$\varphi = \frac{2\pi \cdot n}{\lambda} \cdot p_{l,m}, \qquad l = 0,1,2...(L-1)\,. \tag{2-24}$$

From, eqs (2-23) and (2-24), $p_{l,m}$ will be:

$$p_{l,m} = \frac{\lambda}{n} \cdot \left(\frac{l}{L} + m\right), \qquad l = 0,1,2...(L-1). \qquad (2\text{-}25)$$

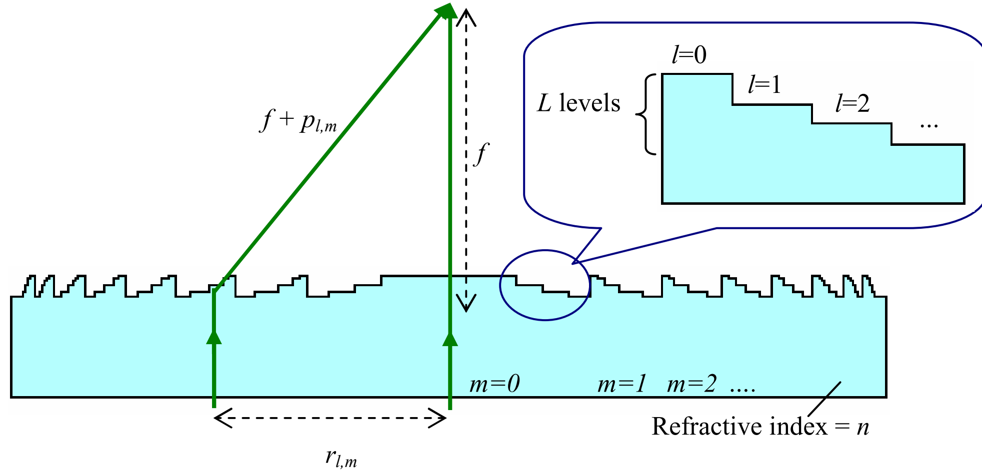

Fig. 2-7 Illustration of a quantized DOE lens.

Since the DOE lens is usually fabricated via standard semiconductor processes, its profile can be regarded as a thin element. Meanwhile, with the validation of paraxial approximation in planar optical systems, the corresponding transverse radius $r_{l,m}$ for the (l, m) level can be derived from the geometry:

$$r_{l,m} = \sqrt{(f + p_{l,m})^2 - f^2}, \qquad l = 0,1,2...(L-1). \qquad (2\text{-}26)$$

It is noted that the $p_{l,m}$ refers to the light path inside the lens. Using the relationship between the depth of level and the phase difference, as shown in Fig. 2-8, the required depth for the lth sub-level, d_l, can be derived:

$$\varphi_l = \frac{2\pi \cdot l}{L} \qquad l = 0,1,2...(L-1). \qquad (2\text{-}27)$$

$$\varphi_l = \frac{2\pi \cdot (n-1) \cdot d_l}{\lambda} \qquad l = 0,1,2...(L-1). \qquad (2\text{-}28)$$

$$d_l = \frac{l \cdot \lambda}{L \cdot (n-1)} \qquad l = 0,1,2...(L-1). \qquad (2\text{-}29)$$

By means of $r_{l,m}$ and d_l, the DOE lens can then be fabricated and operated for a focal length f under the wavelength λ.

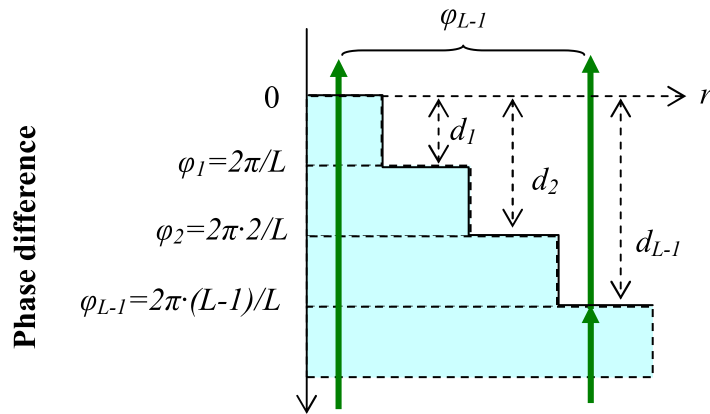

Fig. 2-8 Phase difference between the 0th and the *l*th sub-levels in a DOE lens.

Once the parameters of a DOE are determined, the out-coupling efficiency can be estimated. According to eq. (2-18), the out-coupling efficiency (-1 order considered) is related to the quantization:

$$\eta_{-1} = \mathrm{sinc}^2(1/L) \quad . \tag{2-30}$$

Since this thesis focuses on the efficiency issue, other evaluation factors of a DOE are not discussed herein. People interested in the evaluation of DOEs are suggested to refer to the literature.[4]

2.3 Fabrication techniques

The fabrication techniques of planar optics can be classified into several groups by its feature size, as indicated in Fig. 2-9. Traditional techniques like optical grinding can fabricate devices with the feature size of lager than 1 mm. For the devices with the feature size of 1μm ~ 1mm, diamond machining, excimer laser micro-machining (laser ablation) and those techniques provided by micro-electro-mechanical systems (MEMS), such as photolithography and etching techniques (standard semiconductor processes), are applicable. For a feature size of nano-scale, although some lithography techniques like interference/holography, extreme ultra violet (EUV), X-ray, and focus ion beam (FIB) are available, E-beam lithography dominates the nano-fabrication.

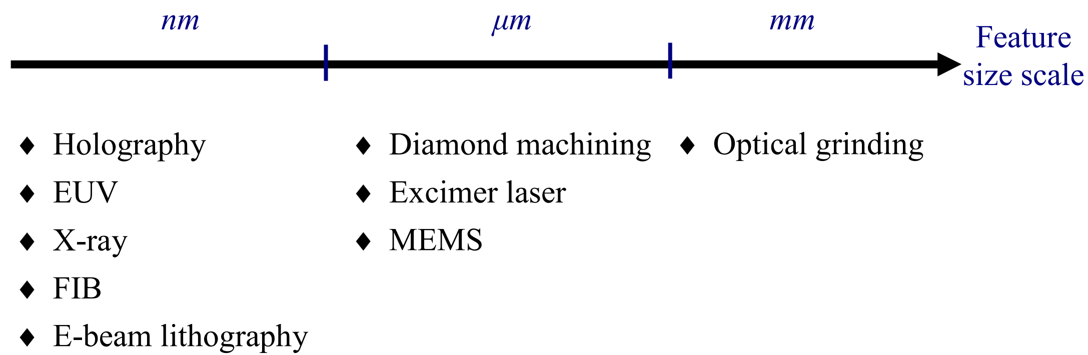

Fig. 2-9 Fabrication techniques of planar optics.

For the mass production of planar optics, the techniques mentioned above can be used for the profile generation and, thus, are suitable for the "test sample" and the master mold fabrications. Then, molding techniques such as lithography-galvanic-forming-molding (LIGA), injection molding or imprint are available to replicate samples. When molding techniques are applied to fabricate the planar optics, some considerations should be highlighted. First, since the plastic replaces the conventional substrate of glass or quartz, the refractive index and the absorbance of plastic, the compatibility with following processes and the temperature tolerance shall be well considered. Second, the achievable feature sizes in the master mold generation and the mold-releasing processes shall satisfy the tolerance requirement.

Among the mentioned fabrication techniques, MEMS, diamond machining and imprint will be emphasized in the following subsections due to their feasibility and maturity.

2.3.1 Micro-electro-mechanical-systems (MEMS)

Due to MEMS' advantage of accurate alignment and one-shot pattern definition, it is widely used for micro-optics fabrication. MEMS can be divided into two main categories: Surface micro-machining (thin film techniques such as sacrificial layer being its main feature) and bulk micro-machining (the etching technique such as the

wet etching being its main feature).[8] For the fabrication of planar optics, bulk micro-machining is exploited more frequently than the other. The typical processes of bulk micro-machining include photolithography and etching. Among the etching techniques, dry etching like reactive ion etching (RIE) provides sharp vertical walls, while wet etching can be isotropic or anisotropic etching, depending on the etchant and the crystal characteristics of substrate. For example, a quantized micro-lens can be fabricated by the MEMS technique with several reiterations of photolithography and RIE-etching. Take the array light-enhancing layer (ALEL), which will be discussed in Chapter 4, as another example. The mold fabrication can be also realized by the MEMS procedures, as shown in Fig. 2-10. First, SiNx is deposited on a silicon substrate as a mask layer. Second, photolithography is applied to pattern definition. Third, taking advantage of the crystal structure of silicon, wet etching can realize the pyramid shape by KOH etchant. Then, by means of RIE, the mask layer of SiNx is removed and the silicon master mold is complete. Finally, applying the fabricated mold to imprint the plastic, such as polydimethylsiloxane (PDMS), one can fabricate an ALEL with the desired profile.

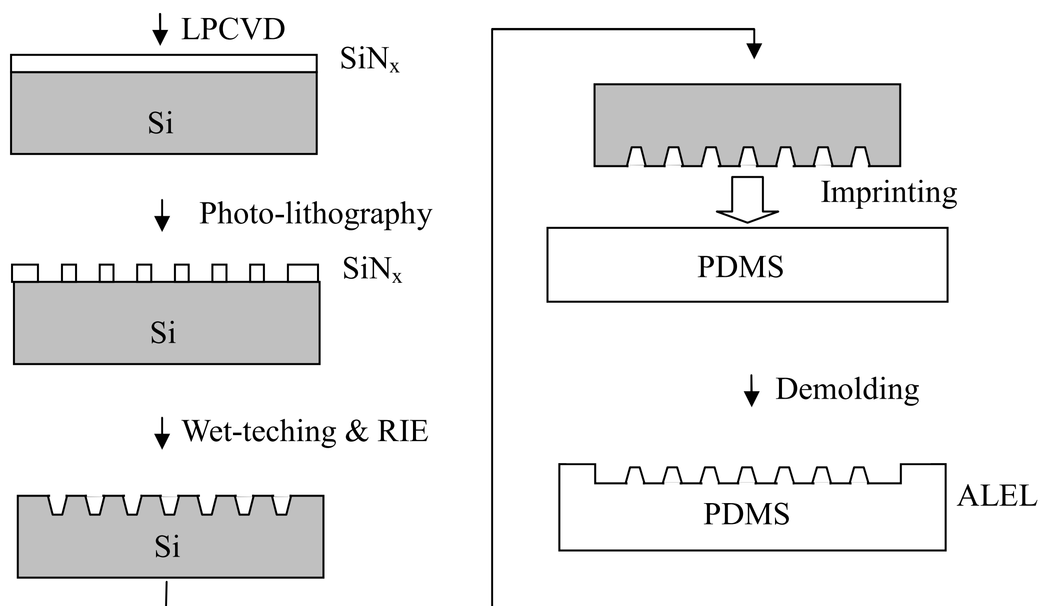

Fig. 2-10 Flowchart of the fabrication of ALEL.

2.3.2 Diamond machining

Diamond machining is another feasible technique for the optics with the size around 1μm ~ 1mm. By using the diamond cutlery and the precise movement stage, the designed profile of planar optics can be carved out with accurate profile and low roughness. The methods of diamond machining include cutting, ruling and turning techniques. For example, the method exploited in fabricating the single pixel of multi-zone light-enhancing layer (MZ-LEL), presented in Chapter 4, is the diamond turning technique. Such a diamond machine comprises of a rotating stage to turn the sample along the X-Y plane and an X-Y-Z stage to move the cutlery to arbitrary positions. The rotation speed and the movement of stages are the critical parameters and controlled by a computer. Although diamond machining works well for the optics of micrometer to millimeter scale, if the size of device is much larger than 1 mm, the fabrication time and cost become uneconomical. As for the device with the size of smaller than 1 μm, conventional diamond machining does not offer reliable resolution or smooth profile. Then, ultra-precision machining with diamond tools, which are able to fabricate surfaces with the form error beneath 0.1μm and roughness beneath 0.01μm, is another candidate.[9]

2.3.3 Imprint

Molding is an efficient approach to realize the mass production. Among the molding techniques, imprint method is an attractive one because of its inexpensive facilities. The imprint technique can produce optics from macro to nano scale. Consequently, the bottleneck does not lie in the achievable feature size of imprint process but in that of the master-mold process. Basically, the imprint can be categorized to three groups: (1) hot embossing, (2) UV imprinting and (3) micro-contact printing, as illustrated in Fig. 2-11.[10] In this thesis, hot embossing was

exploited for the fabrication of ALEL and had performed good results. In the relative research of ALEL, the UV imprinting also provided high-quality samples with convenient process.[11]

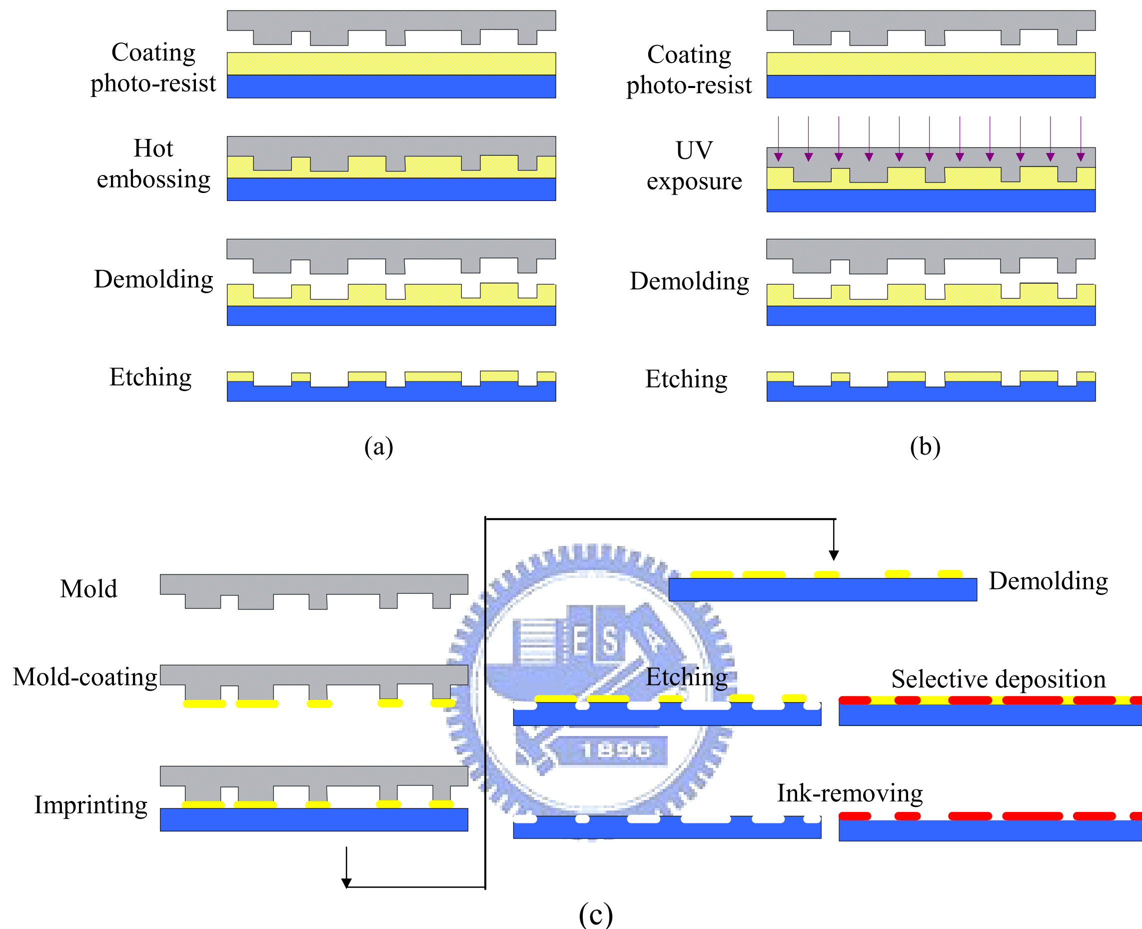

Fig. 2-11 Types of imprint: (a) hot embossing, (b) UV imprinting and (c) micro-contact printing.

2.4 Out-coupling efficiency

Typical planar optics has demonstrated its applications to various areas. However, it has some issues such as aberrations and insufficient out-coupling efficiency. The issue of aberration has been discussed in section 2.1.2, but out-coupling efficiency remains an on-going research topic. In this section, the causes of efficiency issue will be introduced, followed by feasible solutions.

2.4.1 Causes of insufficient out-coupling efficiency

The insufficient out-coupling efficiency of typical planar optics mainly results from the diffraction, the quantization and the reflection. Since the diffraction efficiency can be enhanced by optimizing the profile design, such as blazed DOEs, the discussion in this section focuses on the other two factors. Take a planar DOE as an example. Assume that the device has i reflective components and j quantized DOEs whose efficiencies are η_r and η_{-1}, respectively (the diffraction order is assumed as -1). If the number of quantized levels for every DOE is L, then η_{-1} can be derived from eq. (2-30). Consequently, the out-coupling efficiency of the whole planar optics will be:

$$\eta = (\eta_r)^i \cdot (\eta_{-1})^j . \tag{2-31}$$

Because the quantized profile is usually required to fit the fabrication conditions, the quantization loss can not be avoided thoroughly. Generally, the method for enhancing the efficiency of quantized DOEs is to smooth the surface profile via fabrication techniques, such as gray-scale mask. Since those techniques are beyond the scope of this thesis, people interested in the details are suggested to refer to the published literatures.[12], [13]

On the other hand, the reflection loss is also inevitable. Due to the characteristic of zigzag optical path in typical planar optics, the propagation of light must be confined inside the substrate by the reflective components. When the reflectance of a reflective component is not high enough (e.g. 80%), the resultant out-coupling efficiency will be declined seriously (e.g. 50% after three times of reflections). Therefore, high reflectance is a crucial requirement for the reflective components in typical planar optical systems. Although the target of high reflectance can be realized through total internal reflection designs or dielectric mirrors, they result in restricted system geometries or require complicated coating processes. Hence, the least complex and

most efficient metal coating method is preferred.

In the following subsection, the considerations of metal coating for planar optics will be discussed and one novel method to improve the reflectance will be presented.

2.4.2 Method of improving reflectivity: Composite metal coating

A metallic reflective component in the planar optics has several requirements, including high reflectance, good adherence to the substrate, and good chemical stability. These properties are mainly determined by the materials. A comparison of optical and mechanical properties for metal candidates is listed in Table 2.1.[14] It shows that although Al has excellent adherence to fused silica and superior chemical stability, the reflectance at the operating wavelength (850 nm) is not sufficient. In contrast, Ag shows the highest reflectance at $\lambda = 850$ nm and has a broadband feature with the reflectance of more than 95% throughout the whole visible and near infrared spectrum, but its adherence to fused silica and its chemical stability are poor. Although the shortcomings of Ag might be eased by over-coating a protective Al layer, when the area ratio of the demanded metal (Ag) to the protective layer (Al) is increased, the adhesion of demanded metal becomes weaker.

To achieve a high-reflectance component in the planar optics with excellent adhesion and chemical stability, a novel spatially structured Ag-Al compound coating is demonstrated in our collaborative project.[14] As shown in Fig. 2-12, Ag performs the reflection for planar optical reflective components, while Al serves as the protective layer, the structured under-layer and the bounding pads. The structured Al under-layer is located on the etched ditches which surround the reflective components; as a result, the chemical stabilization can be achieved by anchoring the protective layer to the edges of the etched ditches. Additionally, the bounding pads is distributed sparsely and randomly to uniform the reflectance distribution. Due to the excellent

adherence between Al and fused silica, using Al as the under-layer and the bounding pads can improve the adhesion between the reflective layer (Ag) and the fused silica substrate, thereby protecting Ag from delamination. Meanwhile, because the under-layer and the bounding pads take only a small fraction of the reflective component, the reflectance is almost dominated by Ag and kept in high value.

Table 2.1 Performance parameters of metal films on fused silica for λ = 850 nm

Property		Al	Ag	Au	Cu	Ti
Metal-SiO2	Reflectivity	0.8099	0.9841	0.9829	0.9506	0.5068
Metal-Air	Reflectivity	0.8627	0.9887	0.9877	0.9645	0.6202
Abherence		+	–	–	0	+
Chemical stability		+	–	+	0	+

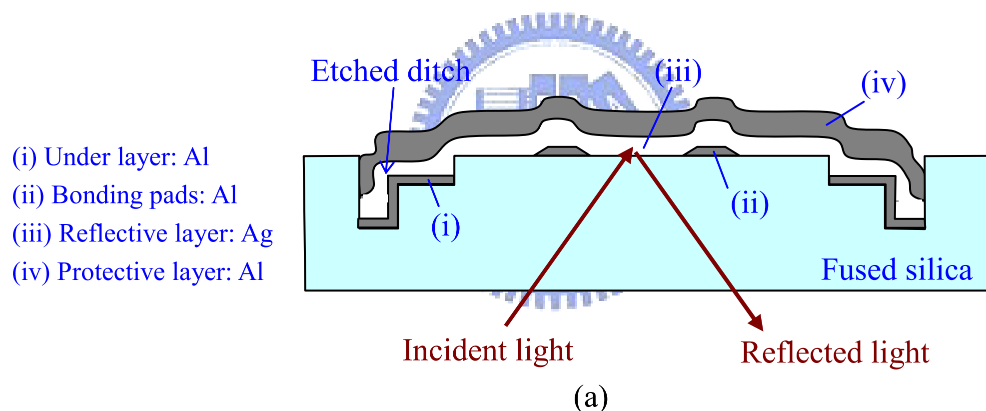

(a)

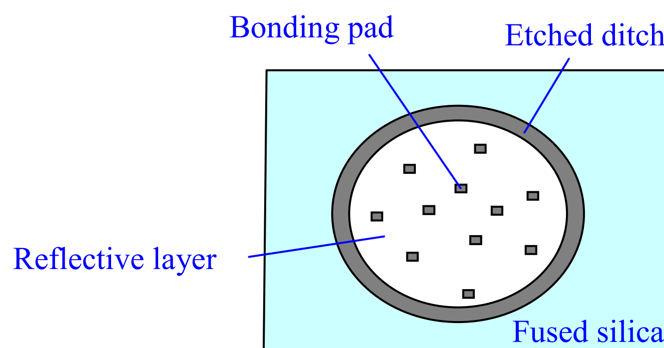

(b)

Fig. 2-12 Ag-Al compound reflector: (a) side and (b) top views.

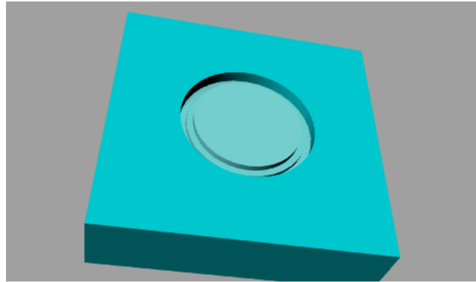

(i) etching the ditch

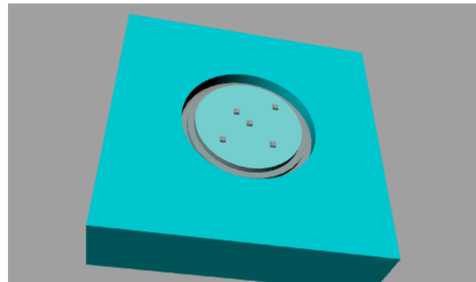

(ii) depositing Al as bonding pads and the under-layer

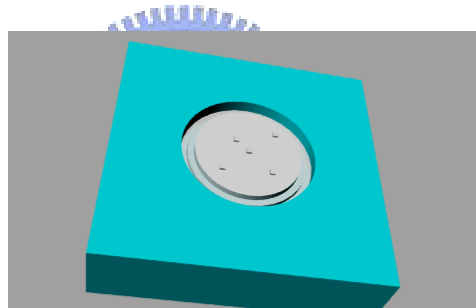

(iii) depositing Ag as the reflective layer

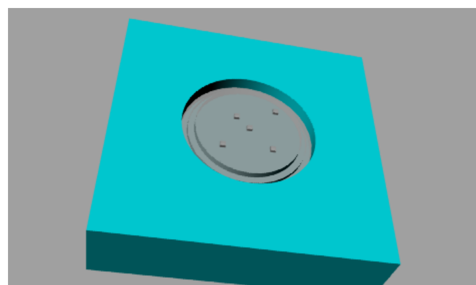

(iv) depositing Al as the protective layer

Fig. 2-13 Fabrication procedures.

A sample was fabricated for demonstration. The fabrication procedures and the fabricated sample are illustrated in Figs. 2-13 and 2-14, respectively. As shown in Fig.

2-14, the central composite reflector was made by the structured Ag-Al compound coating while the Al over-coating was used to make the protective layer with a larger area. The reflectance of Al and that of the composite reflector were measured as 0.807 and 0.980, respectively. Compared with the reflectance of pure Ag (reflectance = 0.984), the composite reflector maintains the high reflectance. The same measurement was repeated two years later. The measured values for Al and the composite reflector were 0.806 and 0.978, respectively. It means that reflectors fabricated by this coating method can stand at normal environmental-condition with little degradation. In another experiment, the composite reflector withstood ultrasonic cleaning for a few seconds without any noticeable damage, whereas the Ag coatings were delaminated completely in the same examination. This result proves that the structured Ag-Al compound coating can improve the adherence of reflectors to the fused silica substrate.

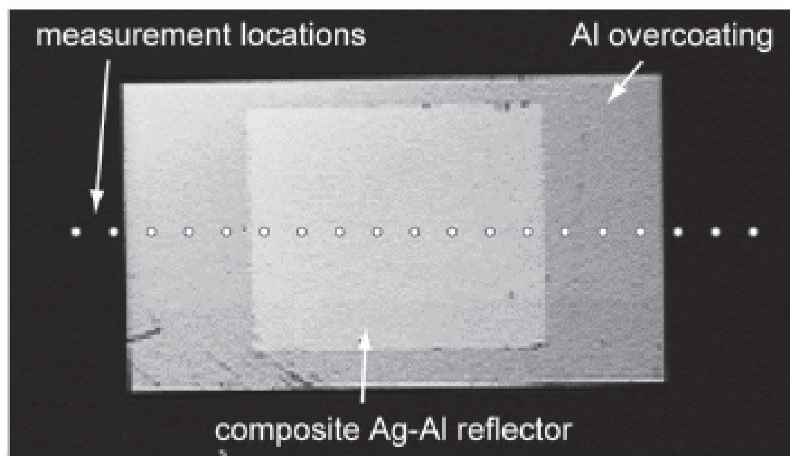

Fig. 2-14 Fabricated Ag-Al compound reflector with the measurement location marks.

Although such a coating method has demonstrated promising results, the sample has not yet passed a standard Scotch tape test. Thus, the proposed device requires further improvement of the adhesion. To further enhance the adhesion, the fabrication

processes need to be improved by several tips. For instance, the adhesion between metal and substrate has been reported to be enhanced by means of the glow discharge to clean the surface of the substrate before the deposition process.[14] Besides, for the reflective components with non-flat surfaces, the adhesion is expected to be further enhanced by optimizing the distribution of the bonding pads.

2.5 Summary

At the beginning of this chapter, a typical planar optics was introduced. To broaden the applications of planar optics, an extended form with the bottom-input and top-output scheme was then proposed to fit the FPD systems. The modeling methods of typical planar optics were given in terms of ROEs and DOEs. ROEs can be modeled by ray optics while DOEs require Kirchhoff and Fresnel diffraction approximations to model the characteristics of thin elements and paraxial propagation, respectively. According to above theories, the design principles of DOEs were then presented. As for fabrication, techniques including MEMS, diamond machining and imprint were emphasized due to their feasibility and maturity. We also investigated the main issues of planar optics and provided probable solutions. In particular, to reduce the inevitable reflective losses in planar optics, we presented a novel structured Ag-Al compound coating to enhance the reflectance of the reflective components, thereby benefiting the out-coupling efficiency of planar optics.

2.6 References

[1] J. Jahns, K.-H. Brenner (eds.), *Microoptics - From Technology to Applications*, Ch13, (2004).

[2] J. Jahns and S. J. Walker, Appl. Opt., **29**, 931-936 (1990)

[3] P. G. Dinesen, J. S. Hesthaven, J. P. Lynov, and L. Lading, J. Opt. Soc. Am. A, **16**, 1124-1130 (1999).

[4] S. Sinzinger, J. Jahns, *Microoptics*, Ch5, Wiley-VCH, (1999).

[5] M. Gruber, Opt. Lett. **26**, 1122-1124, (2001).

[6] Robert E. Fischer and Biljana Tadic-Galeb, *Optical System Design*, Ch3, McGraw-Hill, (2001).

[7] M. Testorf and J. Jahns, J. Opt. Soc. Am. A, **16**, 1175-1183 (1999)

[8] C. R. Yang, "Micro optical devices developed using Si-based Fabrication process and their applications technology", Course 3, Micro-optical system design and application conference, Instrument Technology Research Center, (2005)

[9] http://blog.sina.com.tw/tool/

[10] 蔡宏營,「奈米轉印技術介紹」,中華民國力學學會會訊,104期,92年9月

[11] M. L. Chen, *Design and application of array light-enhanced layer for organic light-emitting diode panel*, Master thesis, NCTU, (2006).

[12] C. Gimkiewicz, D. Hagedorn, J. Jahns, E.B. Kley, and F. Thoma, Appl. Opt., **38**, 2986-2990 (1999)

[13] Z. Zhou and S. H. Lee, Opt. Lett., **29**, 457-458 (2004)

[14] M. Gruber, T. Seiler, and A.C. Wei, Appl. Opt., **45**, 662-667 (2006)